Available online at www.sciencedirect.com
SCIENCE DIRECT®
Journal of Magnetism and Magnetic Materials 302 (2006) 118–121
www.elsevier.com/locate/jmmm

Magnetism origin of Mn-doped ZnO nanoclusters

J.H. Li[a,b], D.Z. Shen[a], J.Y. Zhang[a,*], D.X. Zhao[a], B.S. Li[a], Y.M. Lu[a], Y.C. Liu[c], X.W. Fan[a]

[a]*Key Laboratory of Excited State Process, Changchun Institute of Optics, Fine Mechanics and Physics, Chinese Academy of Sciences, 16 East Nan-Hu Road, Open Economic Zone, Changchun 130033, Peoples' Republic of China*
[b]*Graduate School of the Chinese Acdemy of Sciences, Peoples' Republic of China*
[c]*Center for Advanced Optoelectronic Functional Material Research, Northeast Normal University, Changchun 130024, Peoples' Republic of China*

Received 14 June 2005
Available online 5 October 2005

Abstract

ZnMnO nanoclusters were synthesized by the sol–gel method. The structural and magnetic characters were investigated. The XRD spectrum shows ZnMnO nanoclusters are hexagonal wurtzite structures and a small quantity of $ZnMn_2O_4$ phase is also present in the spectrum. The percentages of Zn and Mn elements in the ZnMnO nanostructure are 97% and 3%, respectively, which are induced from XPS data. EPR spectrum with $g = 1.9961$ shows the signal of Mn^{2+}. The magnetization curve measured at room temperature shows a hysteresis loop. XRD and XPS analyses prove that ferromagnetic ordering arises from $ZnMn_2O_4$ in all probability.

PACS: 75.50.Cc; 75.60.Ej; 68.35.Dv

Keywords: ZnMnO nanoclusters; Room temperature ferromagnetism; Magnetism origin; $ZnMn_2O_4$

1. Introduction

Diluted magnetic semiconductor (DMS) utilizes, synchronously, carrier charge and spin degrees of freedom. Their interaction is expected to exhibit a novel physical character to be applied in new devices. The control of spin-dependent phenomena in electronic oxides or more conventional semiconductors may lead to devices such as spin light-emitting diodes (spin-LEDs), spin field effect transistors (spin-FETs) and so on [1]. DMS is expected to play an important role in materials science and future spintronics. Dietl predicted in 2000, through Zener exchange (Ruderman–Kittel–Kasuya–Yosida-like) mediated by holes in the valence band that the Curie temperature (T_C) of Mn-doped p-type ZnO could be above the room temperature [2]. At the end of 2000, Sato and Katayama–Yoshida's theoretical work of ZnO system using first-principles calculations showed that in the case of Mn doping, the ferromagnetic state is induced by hole doping [3,4].

ZnO is a wide band gap (3.37 eV) semiconductor with large exciton binding energy (~60 meV), which is of great interest for photonic applications. Recently, Mn-doped ZnO has been extensively studied. Many works have shown that Mn-doped ZnO revealed ferromagnetism at $T_C = 30\sim45$ K [5,6], even above room temperature [7,8]. Many methods were employed in the preparation of Mn-doped ZnO, such as PLD [5,7,8], implanting [9], radio frequency magnetron sputtering [10] sol–gel method [8] and so on. The sol–gel method is simple, flexible and economical. Sample composition can be controlled easily by adjusting the different ion proportions in the solution. Here, ZnMnO colloid was successfully synthesized by the sol–gel method in absolute ethanol solutions. By carefully investigating the structural and magnetic characters of the sample, the $ZnMn_2O_4$ phase was thought of as the possible magnetic origination, which shows ferromagnetic property at room temperature.

2. Experiment

ZnMnO colloids were made as follows: 0.1 l of absolute ethanol containing 0.1 M Zn^{2+} and Mn^{2+} was put into a

*Corresponding author. Tel.: +86 431 6176322; fax: +86 431 4627031.
E-mail address: zhangjy53@yahoo.com.cn (J.Y. Zhang).

0304-8853/$ - see front matter © 2006 Elsevier B.V. All rights reserved.
doi:10.1016/j.jmmm.2005.08.025

distillation apparatus so that the solution could undergo reaction under ambient atmospheric pressure and avoided moisture exposure. Zn^{2+} and Mn^{2+} were offered by zinc acetate ($ZnAc_2 \cdot 2H_2O$) and manganese acetate ($MnAc_2 \cdot 4H_2O$), respectively. The solution was refluxed with stirring for 3 h. Next, 4.54 ml tetraethyl ammonium hydroxide ($(CH3)_4NOH$) was added and the ethanol solution was stirred for 30 min at 0 °C. This procedure accelerated the release of OH^- ions and resulted in an immediate reaction to form a stable $Zn_{1-x}Mn_xO$ solution. Acetate was removed by hexane washing, and the resulting $Zn_{1-x}Mn_xO$ powder was annealed at 900 °C in nitrogen ambient for 2 h. Nitrogen gas was kept employed to isolate oxygen in the air.

X-ray diffraction (XRD) was performed on a D/max-rA X-ray diffractometer (Rigaku) using Cu Kα line of 1.5418 Å to determine the crystal structure. X-ray photoelectron spectroscopy (XPS) measurement was carried out on VGESCALAB MK II instrument from Eglish VG Company. Mg Kα X-ray ($hv = 1253.6$ eV) was used as the emission source. The energy scale of the spectrometer has been calibrated with pure C ($E_b = 284.6$ eV) samples, and the pressure in the XPS analysis chamber was 6.2×10^{-7} Pa. Electronic spin paramagnetic resonance (EPR) was performed on JES-FE 3AX spectrometer. Magnetism character was measured using Model 7407 Vibrating Sample Magnetometer produced by Lake-Shore Company.

3. Results and discussion

3.1. Structural property of nanoclusters

Fig. 1 shows the XRD pattern of the sample. Nine prominent peaks with narrow full-width at half-maximum (FWHM) indicate a non-preferential-orientation wurtzite structure. From the pattern, a slight shift of diffractive peaks to small angles shows larger lattice constants. Here, lattice constants a and c were calculated. The resulting values $a = 3.257$ and $c = 5.209$ are a little bigger than those of pure ZnO ($a = 3.25$, $c = 5.2$), which indicates that Mn^{2+} cations with bigger radius (0.89 Å) have entered in the ZnO lattice and replaced Zn^{2+} cations. Mean grain size, 54 nm, was also calculated via Scherrer's formula. Fig. 1 also shows two separated weaker peaks of spinel structure $ZnMn_2O_4$ which correspond to (2 2 4) and (4 0 0) diffractive peak. No other manganese oxide appears in the figure, which indicates that all characters of our sample relate to only ZnMnO nanocluster and $ZnMn_2O_4$.

XPS survey spectrum on the initial surface was produced, as shown in Fig. 2. The elements Zn, Mn and O were found in the spectrum. The Zn $2p_{3/2}$ spectrum exhibits an asymmetry feature with a wide FWHM of

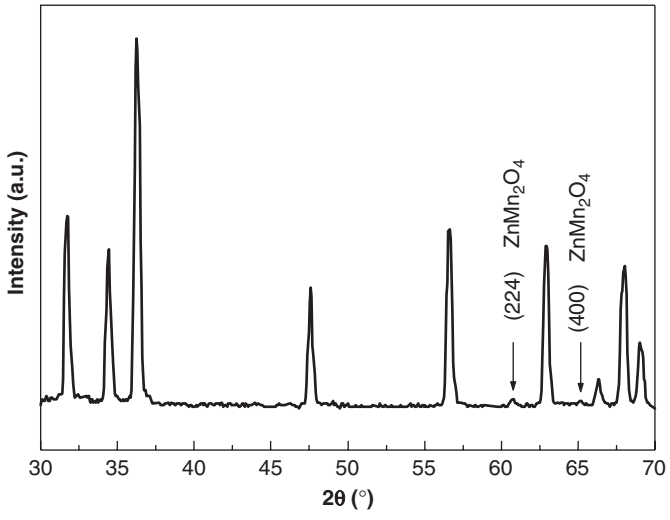

Fig. 1. XRD pattern of the ZnMnO nanoclusters. The arrows are (2 2 4) and (4 0 0) diffractive peaks of spinel structure $ZnMn_2O_4$.

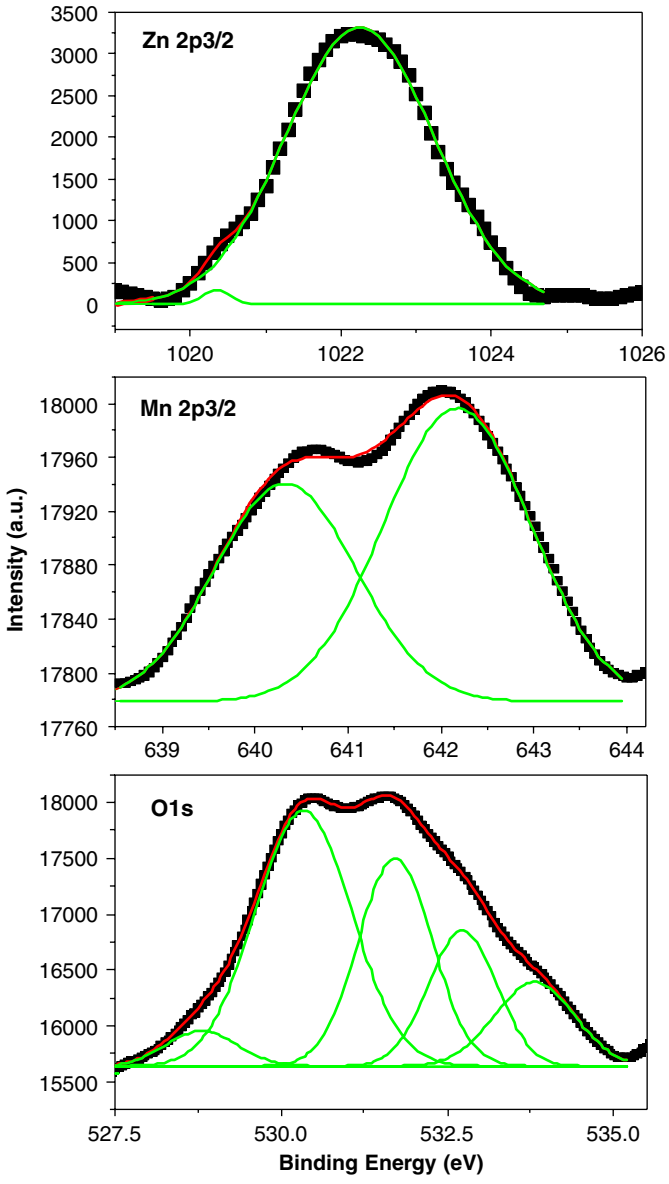

Fig. 2. XPS spectra of ZnMnO nanoclusters. The scattered curves are originally obtained and solid lines figure Gaussian resolving curves.

~1.9 eV, indicating the possibility of existence of multi-component Zn. Gaussian resolving was performed to analyze the component and two peaks were obtained, centered at 1020.36 ± 0.046 and 1022.25 ± 0.006 eV, respectively. Mn with larger ionic radius replacing the lattice Zn of ZnO could result in the increasing binding energy of Zn. So the peak centered at 1022.25 ± 0.006 eV is slightly larger than the value of Zn in the bulk ZnO (1021.4 eV). The peak centered at 1020.36 ± 0.046 eV is thought for the Zn of $ZnMn_2O_4$. In $ZnMn_2O_4$, Mn^{3+} ionic radius (0.66 Å) is smaller than that of Zn^{2+} (0.74 Å), which could result in the binding energy of Zn shifting to the low-energy side. As a result, it is thought that the Zn element in ZnMnO and $ZnMn_2O_4$ consists in the nanocluster together. This result is consistent with the XRD result. The content of two species of Zn induced from the XPS data is shown in Table 1. ZnMnO contains 99% Zn with 1% contained in $ZnMn_2O_4$.

Gaussian resolving was also performed on the Mn $2p_{3/2}$ spectrum to investigate the distributing of Mn element. The result exhibits two kinds of Mn components in our sample, corresponding to 640.33 ± 0.019 and 642.18 ± 0.015 eV. It is well known that, for one kind of element, its ion with a high valence has a larger binding energy than its low valence ion. Therefore, the peak on the high-energy side is considered to correspond to $ZnMn_2O_4$. The component with a binding energy of 640.33 ± 0.019 eV corresponds to ZnMnO. The percentage of two species of Mn is calculated as 41.8% and 58.2%, as shown in Table 1.

Similar to Zn $2p_{3/2}$, the O 1s spectrum is also asymmetric, indicating that multi-component oxygen species were present in the near-surface region. The typical O 1s peak in the surface can be fitted by five nearly-Gaussians centered at 528.8 ± 0.027, 530.34 ± 0.012, 531.72 ± 0.014, 532.73 ± 0.021 and 533.81 ± 0.028 eV, respectively. The peaks centered at about 532.73 and 533.81 eV are due to the chemisorbed oxygen of the surface hydroxyl, $-CO_3$, absorbed H_2O or absorbed O_2. The peak at about 531.72 eV is associated with oxygen-deficient regions in the ZnMnO matrix. The peak at about 530.34 eV is due to the ZnMnO crystal lattice oxygen [11,12]. At present, there is no XPS report of O 1s in $ZnMn_2O_4$. With a view to the above analysis on Zn and Mn, the peak at about 528.8 eV is considered to be the contribution of O 1s of $ZnMn_2O_4$.

According to the former results of XPS, the relative quantitative analysis of each element is completed using the XPS peak area data of different elements and their own elemental sensitivity factor according to the equation: $n(E1)/n(E2) = [A(E1)/S(E1)]/[A(E2)/S(E2)]$, where n is the number of the element atom, E is the element and S is the elemental sensitivity factor. For ZnMnO, the content ratio of Zn and Mn is 97:3. That is, after annealing at 900 °C, only 3% content of Mn entered the ZnO lattice to form $Zn_{0.97}Mn_{0.03}O$ nanocluster and the rest reacted in $ZnMn_2O_4$.

3.2. Magnetic property of nanoclusters

Electron paramagnetic resonance (EPR) measurement was employed to probe the atomic structure of the ground state Mn^{2+} in ZnO. Three types of Mn-related EPR spectra can be distinguished: Mn^{2+} located substitutionally on cation lattice positions in the core of crystals, Mn^{2+} near the surface of the crystals and Mn cluster [13]. The EPR experiment was performed at 9.446 GHz with microwave power of 10,000 mW at room temperature. Fig. 3 displays the broad EPR signal with some unconspicuous shoulders of Mn^{2+}. We obtain the g-value in the Zeeman interaction term to be 1.9961. According to Ref. [13], the broad signal without any six-line structure is typical for exchange-coupled Mn ions. In our experiment, shoulders on the broad signal indicate that there are other

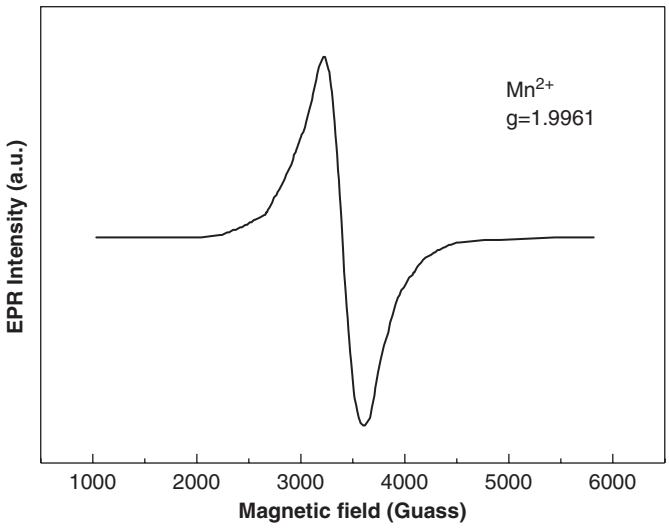

Fig. 3. Room temperature EPR spectrum of ZnMnO nanoclusters. The broad EPR signals with some unconspicuous shoulders of Mn^{2+} are displayed in the figure.

Table 1
Composition and content of three kinds of elements calculated from XPS data

Element	Zn		Mn		O				
PC (eV)	1020.36	1022.25	640.33	642.18	528.81	530.34	531.72	532.73	533.81
FWHM (eV)	0.352	1.965	1.523	1.576	1.062	1.448	1.108	1.022	1.206
Percentage	1	99	41.8	58.2	4.3	42.2	26.2	15.8	11.5

Peak centers (PC), full-width at half-maximum (FWHM) of each peak and percentage of each species are shown in the table.

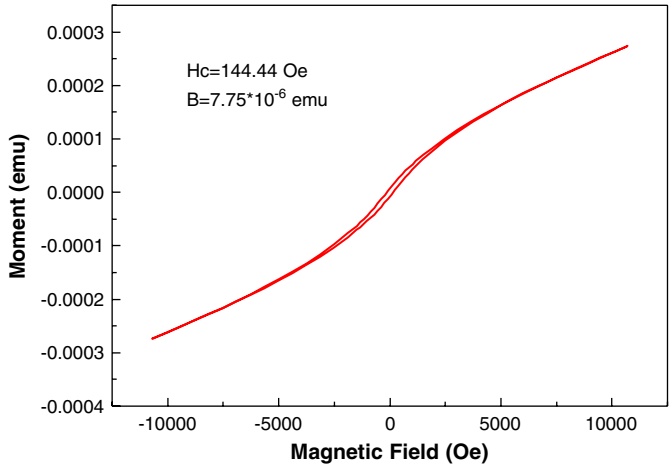

Fig. 4. VSM spectrum of ZnMnO nanoclusters. Room-temperature hysteretic loop shows ferromagnetic ordering.

types of Mn ions in our sample. The value of g is less than that reported for Mn-doped ZnO nanocrystal ($g = 2.002$) but larger than $g = 1.978$ [14]. This indicates that Mn^{2+} substituting Zn^{2+} possibly exists in the interior and near the surface of the crystal together.

To verify the magnetic property, the VSM experiment was performed at room temperature. Fig. 4 shows magnetization curve as a function of the magnetic field. The room temperature hysteretic loop shows ferromagnetic ordering. The coercivity value and the remanent magnetization are 144.44 Oe and 7.75×10^{-6} emu, respectively. DMS behavior has been observed in many reports [5–8]. However, the origin of the ferromagnetism is still in debate, because the substitution of equal-valence ions is electrically equivalent, which is not consistent with Dietl's hole-induced ferromagnetism theory. In addition, in all of the manganese oxide, only Mn_3O_4 is ferromagnetic ordering, and its Curie temperature is around 44 K [15]. But no phase of Mn_3O_4 was observed from XRD and XPS results. This indicates ferromagnetism is not from Mn_3O_4. Another factor for ferromagnetism is $ZnMn_2O_4$ whose T_c is 1298 K [1]. So the well-ordered ferromagnetism could arise from $ZnMn_2O_4$ in our powder in all probability. Even if ZnMnO has ferromagnetism, its quite weak signal may be covered up due to intensive $ZnMn_2O_4$ magnetism—even noise signal of the apparatus itself.

4. Conclusions

We have synthesized the diluted magnetic semiconductor ZnMnO nanocluster by sol–gel method. The nanocluster was found to be a non-preferential-orientation wurtzite structure with a little $ZnMn_2O_4$. The elements Mn, Zn and O were found in the XPS spectrum. Calculation from XPS result indicates $Zn_{0.97}Mn_{0.03}O$ and $ZnMn_2O_4$ co-existing in our sample. EPR pattern with $g = 1.9961$ shows the visible signal of Mn^{2+} and the possibility of three types Mn ions existing in the powder together. Room temperature hysteretic loop shows the coercivity value and the remanent magnetization are 144.44 Oe and 7.75×10^{-6} emu, respectively. The magnetization curve proves that ferromagnetic ordering arises from $ZnMn_2O_4$ in all probability.

Acknowledgements

This work is supported by the National Natural Science Foundation of China, under Grant nos. 60376009, 60278031 and 60176003, the "863" High Technology Research Program in China under Grant no 2001AA311120, the Key Project of National Natural Science Foundation of China under Grant no 60336020, the Innovation Project of Chinese Academy of Science.

References

[1] S.J. Pearton, W.H. Heo, M. Ivill, D.P. Norton, T. Steiner, Semicond. Sci. Technol. 19 (2004) 59.
[2] T. Dietl, H. Ohno, F. Matsukura, J. Cibert, D. Ferrand, Science 287 (2000) 1019.
[3] K. Sato, H. Katayama-Yoshida, Jpn. J. Appl. Phys. 2 40 (2001) 334.
[4] K. Sato, H. Katayama-Yoshida, Jpn. J. Appl. Phys. 2 39 (2000) 555.
[5] S.W. Jung, S.-J. An, G.-C. Yi, C.U. Jung, S.-I. Lee, S. Cho, Appl. Phys. Lett. 80 (2002) 4561.
[6] Y.M. Kim, M. Yoon, I.-W. Park, Y.J. Park, Joung H. Lyou, Solid State Commun. 129 (2004) 175.
[7] P. Sharma, A. Gupta, K.V. Rao, F.J. Owens, R. Sharma, R. Ahuja, J.M. Osorio Guillen, B. Johansson, G.A. Gehring, Nature Mater. 2 (2003) 673.
[8] P. Sharma, A. Gupta, F.J. Owens, A. Inoue, K.V. Rao, J. Magn. Magn. Mater. 282 (2004) 115.
[9] D.P. Norton, S.J. Pearton, A.F. Hebard, N. Theodoropoulou, L.A. Boather, R.G. Wilson, Appl. Phys. Lett. 82 (2003) 239.
[10] D.S. Kim, S. Lee, C. Min, H.-M. Kim, Sh.U. Yuldashev, T.W. Kang, D.Yo. Kim, T.W. Kim, Jpn. J. Appl. Phys. 42 (2003) 7217.
[11] S. Asbrink, A. Waskowska, L. Gerward, J. Staun Olsen, E. Talik, Phys. Rev. B 60 (1999) 12651.
[12] M. Chen, X. Wang, Y.H. Yu, Z.L. Pei, X.D. Bai, C. Sun, R.F. Huang, L.S. Wen, Appl. Surf. Sci. 158 (2000) 134.
[13] H.J. Zhou, D.M. Hofmann, A. Hofstaetter, B.K. Meyer, J. Appl. Phys. 94 (2003) 1965.
[14] R. Viswanatha, S. Sapra, S.S. Gupta, B. Satpati, P.V. Satyam, B.N. Dev, D.D. Sarma, J. Phys. Chem. B 108 (2004) 6303.
[15] Y.Q. Chang, D.B. Wang, X.H. Luo, X.Y. Xu, X.H. Chen, C.P. Chen, R.M. Wang, J. Xu, D.P. Yu, Appl. Phys. Lett. 83 (2003) 4020.